Geophysical Research Letters

RESEARCH LETTER
10.1029/2024GL114258

Dynamic Contributions to Recent Observed Wintertime Precipitation Trends in Mediterranean-Type Climate Regions

Robert Doane-Solomon[1], **Tim Woollings**[1], **and Isla R. Simpson**[2]

[1]Atmospheric, Oceanic and Planetary Physics, University of Oxford, Oxford, UK, [2]Climate and Global Dynamics Laboratory, NSF National Center for Atmospheric Research, Boulder, CO, USA

Key Points:

- Circulation trends are the main cause of the recent observed drying in Central Chile and the US Southwest
- All Mediterranean-type climates exhibit drying independent of circulation trends, which is partially attributable to thermodynamics
- Models suggest internal variability contributes to the drying trends, but some regions show substantial model-observation discrepancies

Supporting Information:

Supporting Information may be found in the online version of this article.

Correspondence to:

R. Doane-Solomon,
robert.doane-solomon@physics.ox.ac.uk

Citation:

Doane-Solomon, R., Woollings, T., & Simpson, I. R. (2025). Dynamic contributions to recent observed wintertime precipitation trends in Mediterranean-type climate regions. *Geophysical Research Letters*, *52*, e2024GL114258. https://doi.org/10.1029/2024GL114258

Received 12 DEC 2024
Accepted 8 JUN 2025

Author Contributions:

Conceptualization: Tim Woollings, Isla R. Simpson
Formal analysis: Isla R. Simpson
Investigation: Tim Woollings, Isla R. Simpson
Methodology: Tim Woollings, Isla R. Simpson
Project administration: Tim Woollings
Resources: Isla R. Simpson
Supervision: Tim Woollings, Isla R. Simpson
Validation: Tim Woollings
Writing – review & editing: Tim Woollings, Isla R. Simpson

© 2025. The Author(s).
This is an open access article under the terms of the Creative Commons Attribution License, which permits use, distribution and reproduction in any medium, provided the original work is properly cited.

Abstract Many Mediterranean-type climates (MCs) have experienced wintertime drying trends since 1979. Using a dynamical adjustment method, we separate the effects of circulation-induced drying trends from other residual trends. Our analysis reveals that circulation trends are the leading cause of the observed drying in Central Chile and the US Southwest, and that models show the drying across Southern Hemisphere MCs is independent of trends in the Southern Annular Mode. All Mediterranean-type climates have exhibited residual drying trends from both internal variability and externally forced thermodynamic processes. Large ensembles suggest internal variability contributes significantly to the observed drying. However, in many regions the observed drying lies outside the ensemble distribution, raising questions about model accuracy.

Plain Language Summary Many Mediterranean-type climates (MCs) have experienced declining winter rainfall since 1979. To understand why this is happening, we use a method to separate the effects of changes in air circulation from other factors. In Central Chile and the US Southwest, changes in air circulation are the main reason for the drying. Even though the Southern Hemisphere MCs are located at similar latitudes, their drying is not linked to global scale patterns of circulation change across those latitudes. Large model data sets suggest natural climate variability plays a key role in the drying, but in some cases, the observed changes are more extreme than the models simulate.

1. Introduction

Mediterranean-type climates (MCs) feature dry summers and wet winters. There are five main subtropical MCs: Central Chile, Southwest South Africa, Southern Australia, the US Southwest, and the Mediterranean itself (Beck et al., 2018; Polade et al., 2017). The annual precipitation cycle in these regions makes water management challenging (Reyes-García & Jofré, 2024; Tortajada et al., 2017), and observations since 1900 indicate a decline in wintertime precipitation in MCs (Seager et al., 2019). In some locations, this decline has accelerated in the 21st century and contributed to extreme droughts, such as the recent "megadrought" in Central Chile since 2010 (Boisier et al., 2016, 2018) and the Cape Town "Day Zero" drought in the late 2010s (Pascale et al., 2020). From model projections, future drying is expected in many of these MCs due to both dynamical and thermodynamic mechanisms (Polade et al., 2017; Seager et al., 2019, 2024).

Large-scale circulation trends have been identified as possible drivers of this precipitation decline. A circulation dipole over the South Pacific has been identified as one cause of the drying over Chile (Garreaud et al., 2020, 2021), and the poleward shift of the westerlies has been implicated across all three Southern Hemisphere MCs (Central Chile, Southwest South Africa, Southern Australia) (Seager et al., 2019, 2024). These zonal wind trends have been associated with a more positive Southern Annular Mode (SAM) over recent decades (Fogt & Marshall, 2020; Marshall, 2003). In the US Southwest, Lehner et al. (2018) found that much of the annual-mean observed drying can be attributed to the development of a ridge over the North Pacific, and circulation variability has also been linked to the late 20th-century decline in wintertime precipitation in the Mediterranean (Kelley et al., 2012).

Thermodynamic "wet-get-wetter, dry-get-drier" arguments have also been used to understand the subtropical precipitation decline driven by global warming (Held & Soden, 2006). However, this framework has limitations due to changing relative humidity and temperature gradients with rising temperatures (Byrne & O'Gorman, 2015). Seager et al. (2019) used a more complex moisture budget in CMIP5 models to analyze the

importance of local dynamic and thermodynamic changes, and found that both were crucial to Southern Hemisphere MC drying in the near future. Given that we generally have greater confidence in the thermodynamic aspects of climate change (Held & Soden, 2006; Shepherd, 2014), it is useful to isolate the precipitation trends caused by dynamics where natural variability can play a relatively important role. Dynamical adjustment methods can do this by quantifying the influence of large-scale dynamics on a target precipitation field (Deser et al., 2016; Lehner et al., 2018). These methods leverage the fact that surface climate variability, such as regional rainfall, is influenced by circulation patterns. Thus, circulation trends and variability affect rainfall trends and variability. However, localized dynamic processes (e.g., convection) and non-dynamic factors (e.g., soil moisture, humidity) can also contribute, forming the residual influences. Multiple different dynamical adjustment methods exist (Sippel et al., 2019), including constructed circulation analogs (CCAs). These have shown use in understanding European climate trends (Deser & Phillips, 2023) as well as Northern Hemisphere precipitation trends (Guo et al., 2019).

In this study, we use CCAs to quantify the contribution of changes in the large scale circulation to the observed wintertime precipitation decline in MC regions over the satellite era. We make use of large ensemble (LE) data from three CMIP6-class models and an atmosphere-only (AMIP) ensemble plus observations and reanalysis. As with multiple other studies (Deser & Phillips, 2023; Deser et al., 2016; Guo et al., 2019; Lehner et al., 2018), we use the LE data to understand the contribution of external forcing and internal variability to the observed precipitation trends.

2. Data and Methods

2.1. Observational Data Sources

We use precipitation gauge data from the Climatic Research Unit Time Series (CRU-TS) version 4.07 (Harris et al., 2020). This is a 0.5° × 0.5° gridded data set of total monthly precipitation from 1901 to 2022. We also use the satellite-gauge product from the Global Precipitation Climatology Project (GPCP) (Adler et al., 2003) for total monthly precipitation from 1979 to 2022, remapped to the same 0.5° × 0.5° grid. This allows for a reliable observational estimate in regions with sparse gauge coverage. We use 0.5° × 0.5° monthly mean sea level pressure (SLP) data from the ERA5 reanalysis (Hersbach et al., 2023). We also use a land-sea mask from ERA5 when calculating all precipitation averages with a 50% land threshold.

2.2. Model Data Sources

We compare the observed trends to three large ensemble (LE) data sets from the Multi-Model Large Ensemble Archive (Deser et al., 2020). The first is a 100 member ensemble from the Community Earth System Model version 2 (Rodgers et al., 2021) (nominal 1.0° resolution). The second is a 50 member ensemble using the MPI-ESM1.2-LR model (Olonscheck et al., 2023), (nominal 1.5° resolution). The third is a 50 member ensemble produced by the Swedish Meteorological and Hydrological Institute using the EC-Earth3 model (SMHI-LENS, Wyser et al. (2021)) (nominal 1.0° resolution). Hereafter, these LEs are referred to as CESM, MPI and EC-Earth respectively. Each of these LEs is forced with CMIP6 historical forcing from their initialization in 1850 until 2014, and are forced with the SSP370 scenario from 2015 to 2100. The CESM LE includes 50 members with smoothed biomass burning emissions instead of the CMIP6 default, but as no significant trend differences were found, all 100 members were combined in this study. These models were selected for their consistent forcing (SSP370), ensemble size (≥50 members), and contrasting SH jet biases (Simpson et al., 2020). We also compare the observations and LEs to the 10-member CESM2 Prescribed SST AMIP Global Ensemble (referred to here as CESM-AMIP) to isolate the influence of observed SSTs on the precipitation trends, using data from 1979 to 2019 (Phillips & Simpson, 2024).

2.3. Dynamical Adjustment Using Constructed Circulation Analogs

A dynamical adjustment framework is used to isolate the contribution of large-scale dynamics on rainfall. We use a constructed circulation analog method similar to Deser et al. (2016) and Lehner et al. (2018). The general method is described in more detail in Deser et al. (2016), but we give an explanation below, with Figure S1 in Supporting Information S1 as an example. We use SLP instead of 500 hPa geopotential height as our dynamical variable due to its better performance in capturing precipitation variance (see Figure S2 in Supporting Information S1).

Using wet season months only, we calculate SLP and precipitation monthly anomaly fields versus the 1979–2022 climatology (see Section 2.4 for an explanation of the domains and wet seasons). For each "target month" (e.g., July 2021 in Figure S1 in Supporting Information S1), we find the N_a wet season months in our data set which exhibit the most similar pressure anomalies, using cosine-latitude-weighted total Euclidean distance. A random subsample of size N_s is selected without replacement from these N_a analog months to avoid overfitting. Next, we regress the target month pressure field onto each of the N_s pressure analogs. This gives us a corresponding regression coefficient β_i for each analog month $i \in [1, N_s]$. The target month's pressure field is then reconstructed as a weighted sum of these analogs, using the coefficients β_i derived from the regression. The reconstructed pressure field closely matches the original (Figures S1b vs. S1c in Supporting Information S1).

Next, we select the precipitation anomaly fields from the same N_s subsampled analog months. We reconstruct the target month precipitation as the weighted sum of the analog monthly precipitation anomalies multiplied by *the same β coefficients from the pressure linear regression*. This way, we estimate the SLP influence on the precipitation anomaly field (Figure S1e in Supporting Information S1). This procedure is repeated N_r times, and the average is taken to obtain the dynamic anomaly field. Subtracting this from the total anomaly yields the residual anomaly. By repeating this with each month as the target, we create two timeseries of dynamic and residual precipitation. In this study, we choose $N_a = 50, N_s = 30$, and $N_r = 100$: this uses a similar proportion of the overall data as analogs as in Deser et al. (2016).

Precipitation trends are calculated using OLS regression: performing this for each LE member gives a spread in trends. We interpret the LE mean to be an estimate of the forced trend and the spread of trends as the internal variability. The difference between the observations and the model mean is interpreted as the contribution of internal variability to the observed trend, although model and observational errors could contribute. 95% confidence intervals are estimated by bootstrapping with 1,000 resamples.

2.4. Regions and Seasons Studied

We examine five subtropical Mediterranean-type climates, shown in red boxes in Figure 1a. The regions are:

1. The US Southwest ("USSW": 123°W–105°W, 32°N–39°N)
2. The Mediterranean ("Med": 10°W–40°E, 30°N–45°N)
3. Central Chile ("Chile": 74°W–70°W, 30°S–42°S)
4. Southwest South Africa ("SWSA": 18°E–21°E, 32°S–35°S)
5. Southern Australia ("SAus": 114°E–142°E, 30°S–39°S)

These contain Köppen Csa- and Csb-type climates as shown in Seager et al. (2019), however in contrast to Seager et al. (2019) we do not mask by these Köppen regions due to their small size and use precipitation from all land points within the red boxes. We use the same eastern boundary in Southern Australia as Polade et al. (2017) to include the CSb-type climate found near 140°E. We choose to analyze winter months in the peak of the wet season. These are DJFM for USSW, NDJ for Med and MJJA for Chile, SWSA and SAus (see Section 3.1 and Figure 1). We also only use the analogs from 1979 to 2022, due to unreliable Southern Hemisphere SLP data before the satellite era (Fogt & Marshall, 2020; Jones & Lister, 2007). For the SAM index, we calculate the longitudinal-mean SLP difference between 40°S and 65°S. We then use the unnormalized anomaly (the method of Velasquez-Jimenez and Abram (2023)) as our SAM index. According to convention, we take a positive SAM index to be higher-than average pressure at 40°S and lower-than-average pressure at 65°S.

3. Results

3.1. Precipitation Climatology and Trends

We begin by analyzing the CRU-TS and GPCP climatological monthly precipitation of the five regions shown in Figure 1, which also shows the average monthly precipitation for each region and the interquartile range. In USSW (Figure 1b), we see two annual wet seasons: in DJFM and in July–August. We focus on the wintertime wet season of DJFM due to the convective nature of the summertime wet season (Adams & Comrie, 1997; Barlow et al., 1998; Carleton et al., 1990) which is not well captured by dynamical adjustment. In the Mediterranean (Figure 1c), we see a smooth annual cycle peaking in December with a minimum in July. Defining a strict wet season is more difficult here, but months NDJ all have mean precipitation of over 50 mm/month in CRU-TS and 60 mm/month in GPCP. We therefore take this to be the wet season. In all three Southern Hemisphere regions

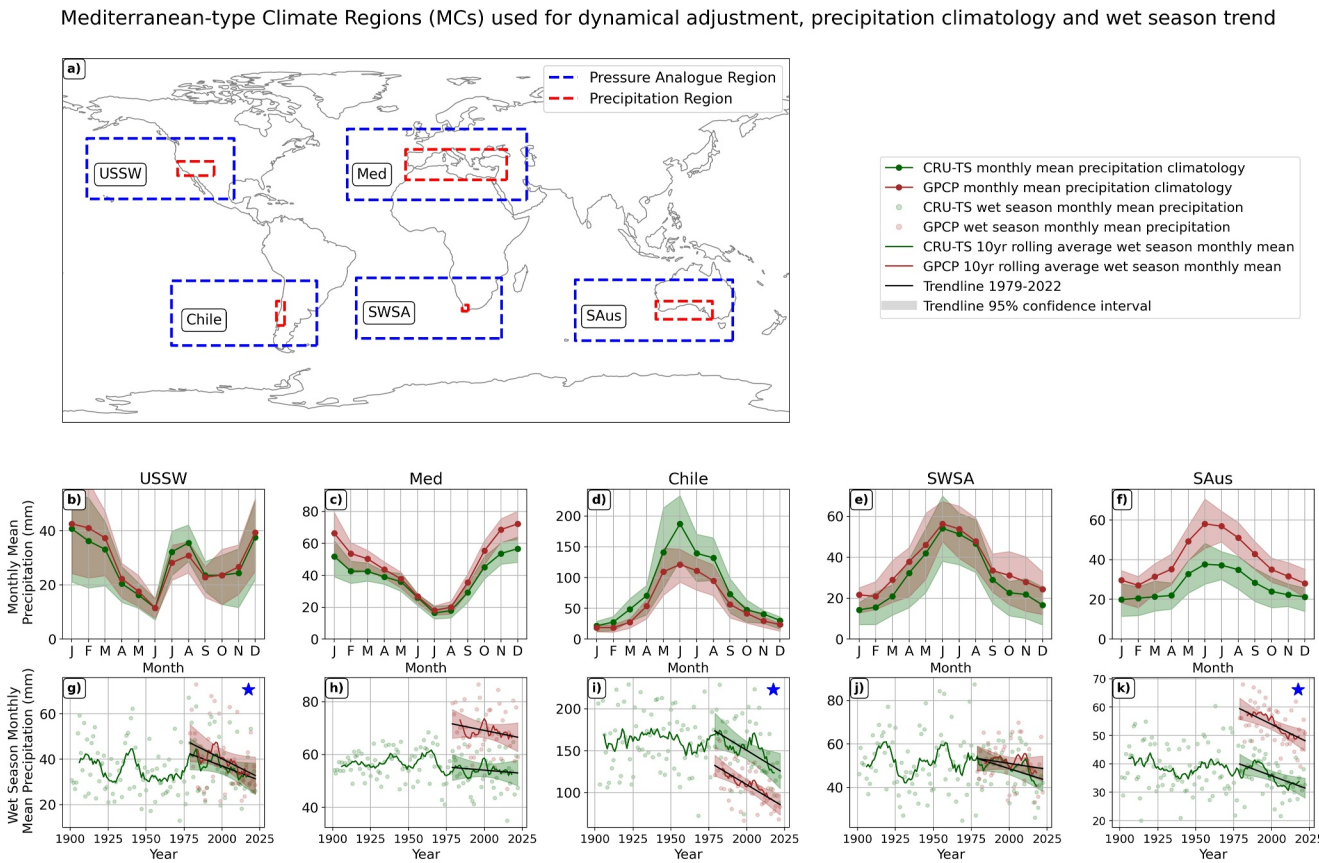

Figure 1. (a) shows the regions used. Red boxes show the region over which precipitation averages are calculated, and blue boxes show the domains for the pressure analogs. The *y*-axis range is different for each region. (b–f) Show the observed climatology (CRU-TS: 1901–2022, GPCP: 1979–2022) of monthly mean precipitation in the 5 MCs. Shading shows the interquartile range of the monthly rainfall. (g–k) Show timeseries of the wet season mean monthly precipitation in the 5 MCs with a 10-year rolling average and the trend over the satellite era (1979–2022, black, with 95% confidence interval shaded in color, regions with significant trends indicated by a blue star).

(Figures 1d–1f), we see a similar seasonal cycle in precipitation with a peak in July and a minimum in the summer months. By examination, we define the wet season to be MJJA for all three regions.

The timeseries (Figures 1g–1k) reveal that all MC regions have experienced decadal variability in addition to a wet season drying trend over the satellite era (1979–2022). This trend is most pronounced and has the highest confidence in Central Chile (Figure 1i), while it is least pronounced and has low confidence in the Mediterranean (Figure 1h). In the three Southern Hemisphere regions (Figures 1i–1k), since approximately 2010, the CRU-TS data shows decadally averaged precipitation has been lower than at any point in the 20th century. Similarly, in the Northern Hemisphere regions (Figures 1g and 1h), recent decadally averaged precipitation is at the lower end of the distribution considering years going back to 1900. These recent lows across all five MCs motivate a deeper investigation into the drivers of this drying.

3.2. Dynamical Adjustment Results

We now apply the dynamical adjustment framework to the precipitation trend in these regions, using both observations (ERA5/CRU-TS, ERA5/GPCP) and the three large ensembles (CESM, MPI & EC-Earth). As an example, we initially focus on the precipitation trends in Central Chile (Figure 2). In the CRU-TS observations we see a total drying trend in Central Chile of -1.13 ± 0.74 mm/month/year in MJJA over the period 1979–2022 (Figure 2k), and -1.24 ± 0.56 mm/month/year in GPCP (Figure 2l). In Figures 2a and 2f, we split the total CRU-TS trend into dynamic and residual trends, and likewise for GPCP in Figures 2b and 2g. We see that in both observational data sets, the dynamic trend is stronger and more spatially widespread than the residual trend. This, along with the high pressure trend west of Chile shown in the contours (Figures 2a and 2b) provides strong

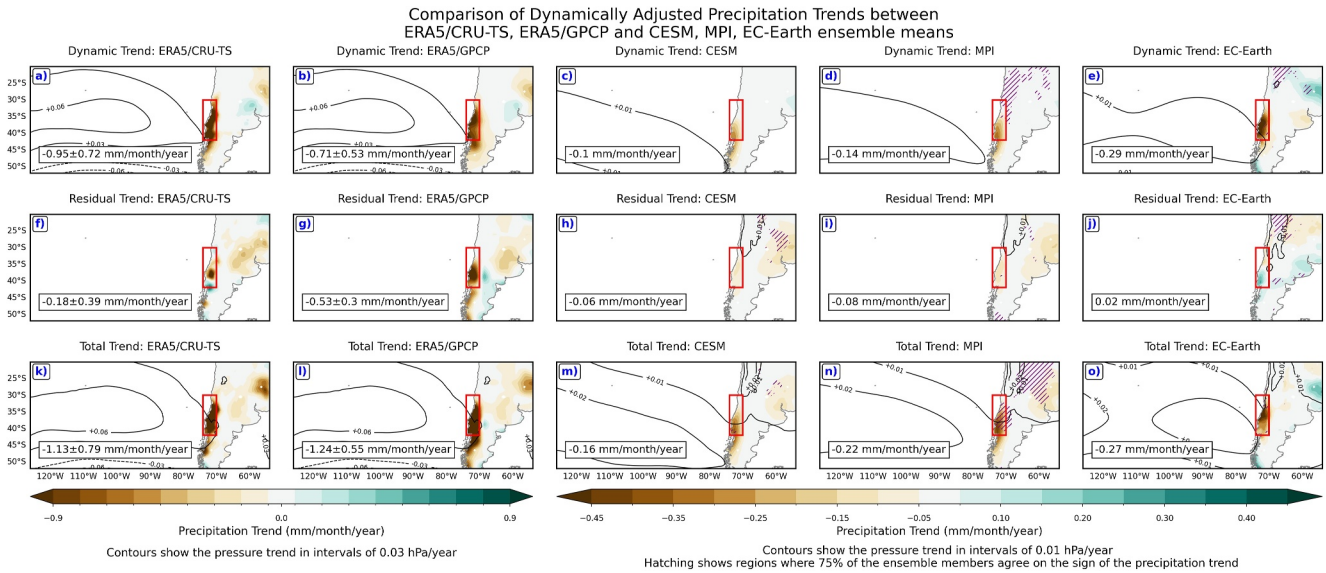

Figure 2. Central Chile precipitation trends: the top row shows dynamic trends, middle row residual trends, and bottom row total trends. The left columns show observed ERA5/CRU-TS and ERA5/GPCP trends; the right columns show ensemble mean trends for CESM, MPI, and EC-Earth. Precipitation trends are shown in color and SLP trends as contours (0.03 hPa/year for observations, 0.01 hPa/year for ensembles; solid = positive, dotted = negative). Purple hatching shows where 75% of ensemble members agree on the sign of the trend. The subplot text shows the average trend over the red MC region (with 95% confidence intervals for observations).

evidence the observed drying trend in Chile is mostly associated with circulation anomalies in the Pacific to the west of Chile, in agreement with Garreaud et al. (2020).

In the ensemble mean (forced) trends of the LEs, we also see a negative total precipitation trend (Figures 2m–2o). It is shifted approximately 5° further south, with little drying north of 35°. In addition, the magnitude of the drying trend is significantly lower than in the observations, ranging from −0.16 to −0.27 mm/month/year compared to over −1 mm/month/year in observations. However, the dynamical adjustment also shows that a substantial portion of these forced trends are associated with circulation trends. CESM, MPI and EC-Earth attribute over half of the total ensemble mean precipitation trend to dynamics. CESM and MPI both show a residual drying contribution, however EC-Earth simulates a small residual wetting.

Next, we extend this analysis to all five MC regions and the distribution of LE trends. Maps for the other MCs similar to Figure 2 are available in Figures S3–S6 in Supporting Information S1. The results from all the regions are summarized in Figure 3. Beginning with Central Chile (Figure 3c), we see that the CRU-TS and GPCP overall trends are completely outside the distribution of trends in the CESM and MPI LEs, and toward the bottom end of the EC-Earth ensemble (right group of violin plots). The results are similar for the observed dynamic trends (left group). The residual trend is also below the mean of the ensembles, and completely outside for GPCP. We note that some ensemble members show wetting, highlighting the ability of internal variability to override the forced trend (see Figures S7 and S8 in Supporting Information S1 for evaluation of the models' internal variability).

In SWSA, the observed total drying trends are consistent with the ensembles, though again on the drier end of the distributions. SWSA exhibits a dynamic wetting in both observational data sets. These are mostly consistent with the ensembles, though the mean (forced) response across all three LEs appears to be a drying. However, there is a statistically significant residual drying in the observations, at the drier edge or completely outside the LEs. In SAus, we again see a large ensemble spread. The dynamic, residual and total trends all show a drying on average, with varying significance. Both observational estimates of the observed dynamic and residual trends are at the drier end of the ensembles, and the total precipitation trends from both CRU-TS and GPCP are slightly outside the distribution of trends from MPI and EC-Earth.

In both Northern Hemisphere regions, the CRU-TS and GPCP area-averaged precipitation trends are similar, although the spatial patterns differ somewhat in the Mediterranean (see Figure S9 in Supporting Information S1 for further discussion). In both USSW and Med the total observed trends are consistent with the ensembles but again toward the drier end, despite substantial inter-model variability. The observed dynamic trends are well

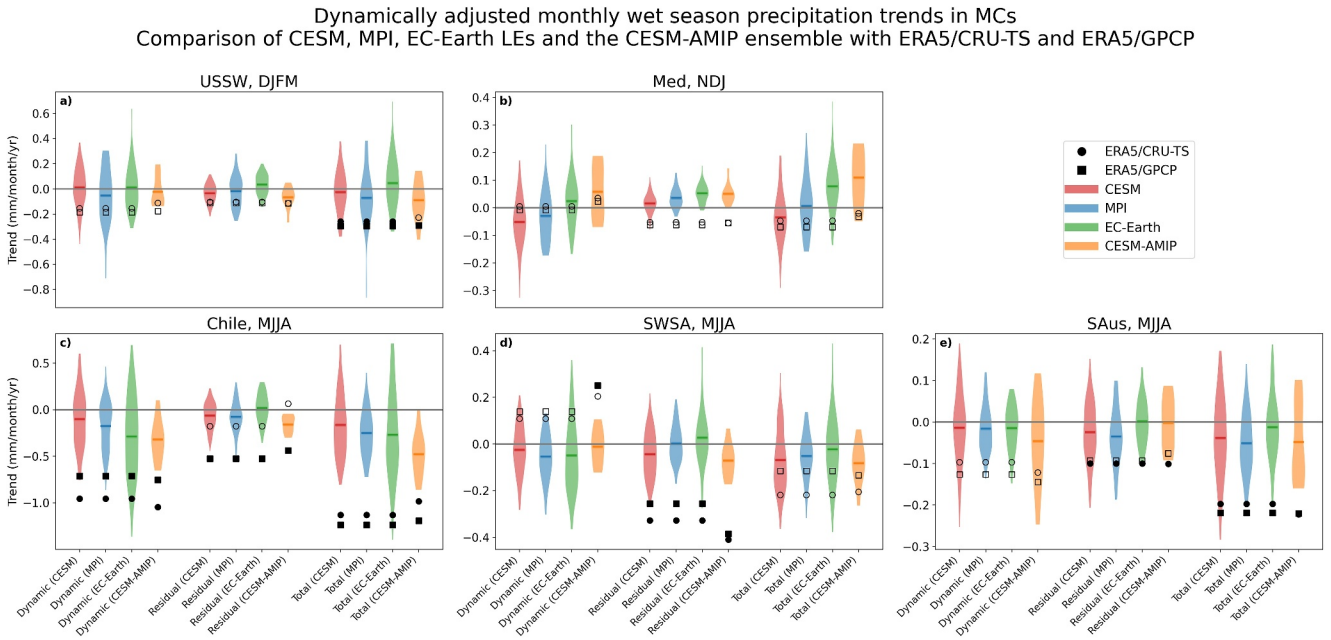

Figure 3. Dynamically adjusted wet season precipitation trends for CESM, MPI, EC-Earth LEs (1979–2022) and the CESM-AMIP ensemble (1979–2019) compared to ERA5/CRU-TS and ERA5/GPCP observations. Subplots (a–e) represent USSW, Med, Chile, SWSA, and SAus. The violins show dynamic, residual, and total trends for the CESM, MPI, EC-Earth, and CESM-AMIP ensembles, with the means as horizontal lines. Observed trends (ERA5/CRU-TS, ERA5/GPCP) are filled if significant at 95% confidence. The gray line indicates zero trend.

within the distributions, but in Med, the residual drying is outside all but CESM. We note the lack of statistical significance in the overall observed Mediterranean drying, in contrast to the strong drying seen in Seager et al. (2024). High levels of NAO multidecadal variability and our choice of a different time period may explain this discrepancy (Harvey et al., 2023; Seager et al., 2019).

In summary, across all five regions we see an observed total drying trend, with statistically significant trends in USSW, Chile and SAus. All three LEs simulate a total drying trend in the ensemble mean, except for EC-Earth in USSW and Med. In the observations, all regions show a residual and dynamic drying trend except for the dynamic trends in Med and SWSA. We see statistically significant dynamic drying in Chile. Dynamic trends contribute the largest fraction of the observed and modeled trends in Chile and USSW, while residual and dynamic are approximately equal in SAus. Most notably, the observations are often toward the edges of the ensemble spread, and sometimes entirely outside it. Using the JRA-3Q reanalysis (Kosaka et al., 2024) to perform the dynamical adjustment instead of ERA5 gave similar results (not shown).

3.3. Contribution of External Forcing

Figure 4 shows the contributions of forced dynamic, forced residual, internal dynamic, and internal residual trends to the total observed drying in the five MCs, calculated as described in Section 2.3. In general it appears internal variability dominates over forced contributions, however all regions show a large internal residual, raising concerns about the models' ability to accurately simulate the forced residual component. The Southern Hemisphere regions exhibit negative forced dynamic trends, but these are smaller in magnitude than the internal dynamic trends. In USSW the modeled forced responses are weak and inconsistent, but internal variability can produce drying trends as large as the observed. The Mediterranean is the only region where forced trends are comparable to internal variability, though the internal residual remains the largest contributor to the observed drying.

3.4. Influence of the Southern Annular Mode (SAM) and Observed SST Trends

The SAM has been demonstrated to have influence over precipitation variability in the midlatitudes (Gillett et al., 2006; Lim et al., 2016; Meneghini et al., 2007). In Figure S10 in Supporting Information S1 we show the

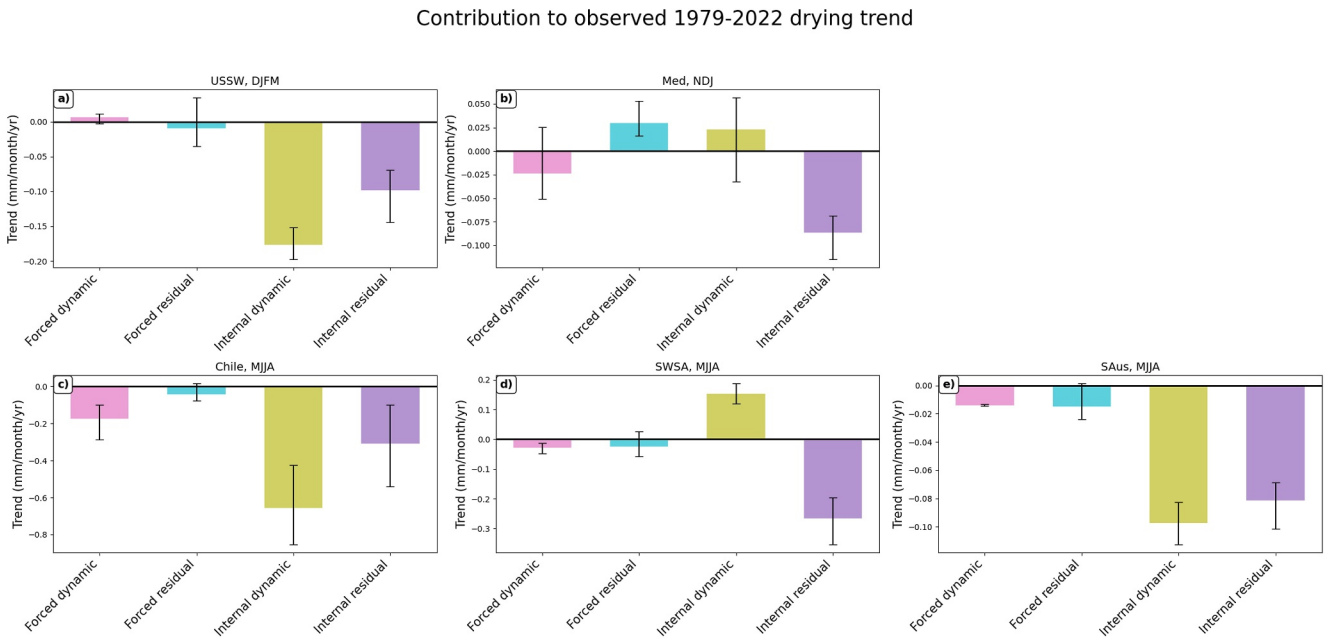

Figure 4. Contribution to observed precipitation trends in MCs (1979–2022) for regions USSW, Med, Chile, SWSA, and SAus. The bars show the multimodel mean trends. Error bars for the forced components represent the maximum and minimum ensemble mean trends. For the internal components, they show the difference between the maximum observed trend (CRU-TS/GPCP) and the minimum model mean trend (CESM/MPI/EC-Earth), and vice versa.

relationship between the modeled SAM trend and dynamic precipitation trend in MJJA for the Southern Hemisphere MCs. The SAM explains 20% of the variance in trends in dynamic precipitation in Chile but 1% in SWSA and SAus. This suggests (in line with Seager et al. (2019)) that SAM trends may only have had a weak influence on recent wintertime drying in MCs, even if the SAM is thought to be important in the future (Lim et al., 2016). Additionally, the large spread in simulated SAM trends is further evidence of a weak forced circulation response compared to internal variability.

To understand the influence of observed SST trends, in Figure 3 we also compare the CESM LE with the CESM AMIP ensemble, using data from 1979 to 2019. In Chile (Figure 3c), the mean dynamic, residual and total trends are significantly closer to observations in the AMIP ensemble than in the LE. However, prescribing observed SSTs does not change the fact that the observed trends are still outside the model distribution. The spread is smaller, although this is possibly due to having 10 members in the AMIP ensemble compared to 100 in the LE. In USSW and SWSA (Figures 3a and 3d) the mean drying from the AMIP ensembles is only slightly closer to the observations than the large ensemble. In SAus (Figure 3e) there is large variability in the AMIP ensemble: a slightly drier mean dynamic drying is offset by a residual drying mean that is further from observations than in the LE. Finally, in the Mediterranean (Figure 3b), the AMIP ensemble suggests both a dynamic and residual wetting.

4. Discussion

In this study, we have shown the importance of both large-scale dynamics and other, residual processes to the observed wet season drying trends in five Mediterranean-type climate regions. All five regions have exhibited a recent drying trend, with the models suggesting a component of this is forced in the Southern Hemisphere, although that forced component is relatively small. Dynamic precipitation trends are particularly large in Central Chile and also contribute significantly to the drying in the US Southwest and Southern Australia. All five regions also show negative residual trends. The observed precipitation trends are at the edge or outside of the ensemble range in many cases, in particular in the Southern Hemisphere.

These observed trends are not always consistent with the ensemble means (e.g., dynamic trends in SWSA), suggesting a substantial role of internal variability. However, this assumes the LEs accurately simulate the forced response and variability, which appears unlikely. For instance, the three LEs disagree on the sign of the forced dynamic trend in both Northern Hemisphere regions, and of the forced residual in all regions except the

Mediterranean. Therefore, the decomposition into forced and internally driven components should be treated with caution in these cases. Seager et al. (2024) also find larger MC wintertime precipitation declines in CRU-TS than in models, which aligns with our findings despite using slightly different time periods, seasons, and regions. We therefore believe that these models should be more closely examined for their representation of mechanisms involved in subtropical drying.

The existence of the residual drying in all five regions motivates the question of its physical interpretation. Residuals have previously been attributed to thermodynamic effects from radiative forcing (Guo et al., 2019) in line with the wet-get-wetter, dry-get-drier principle (Held & Soden, 2006). O'Reilly et al. (2017) caution that the residuals may contain smaller-scale dynamic processes and sub-monthly circulation variability: Parker and Gallant (2022) find that sub-monthly rainfall variability is critical for controlling drought in Southern Australia. We agree with these assessments, and add that any upper- or mid-level dynamic changes independent of SLP that influence precipitation are not reflected in the dynamic component. Additionally, we highlight that coupled dynamic-thermodynamic change is also included in the residual component. For example, nonlinear interactions between humidity trends and pressure trends will not show up in the dynamic trend but in the residual trend instead, and an interaction between a forced humidity trend and an internal pressure trend will end up in the internal residual. Due to these nonlinearities, we argue that the internal dynamic component does not capture all of the true dynamic variability and that the forced components are potentially an underestimate of the true anthropogenic effects. Indeed, the large negative internal residuals in all five regions may imply that the models or the framework are underestimating the forced residual in particular: future work is necessary to understand the physical processes influencing the residual drying.

The CCA framework used here provides an alternative method of understanding the physics of precipitation change in MCs compared to the direct moisture budget analysis used in Seager et al. (2019). That study finds that a large component of near-term future drying in Central Chile is driven by the change in mean flow moisture divergence, and that SAM trends are not a major driver of the drying. Our analysis also indicates that over the recent observed period dynamic change has been the dominant factor in both observations and models and that the hemispheric SAM trend has only had a weak contribution. Indeed, the dynamic drying in Chile and Australia contrasts with the dynamic wetting in South Africa. This is despite the SAM being the dominant mode of atmospheric variability in the Southern Hemisphere (Fogt & Marshall, 2020; Hessl et al., 2017; Marshall, 2003) and this variability being overestimated in CMIP6 models (Coburn & Pryor, 2021). Woollings et al. (2023) find a significant strengthening in ERA5 of JJA zonal wind over South Africa but nowhere else, potentially consistent with our finding of dynamic wetting, and further suggesting weak SAM-congruent trends. Therefore, we argue that the recent MJJA dynamic drying is driven by regional high pressure patterns unrelated to the SAM (see Waugh et al. (2020) for related wind trends), as shown in Figure S11 in Supporting Information S1. We also note that the consistent magnitude of dynamic drying between the models in the Southern Hemisphere regions suggests that the differing Southern Hemisphere jet biases in these models (Simpson et al., 2020) likely have little influence.

Additionally, residual precipitation trends in models are also inconsistent with observations in Southwest South Africa, the Mediterranean, and Central Chile, raising questions about the models' fidelity beyond atmospheric dynamics. CMIP6-generation models are known to have opposite-signed Pacific SST trends to observations, simulating a weakening of the zonal SST gradient whereas observations show a strengthening unlikely due to internal variability (Seager et al., 2022; Wills et al., 2022). USSW and Chile precipitation is known to be modulated by these tropical Pacific SSTs (Campos & Rondanelli, 2023; Montecinos & Aceituno, 2003; Wang & Kumar, 2015), likely having implications for the forced precipitation trends in these regions as explored by Alessi and Rugenstein (2024). Our AMIP analysis finds that recent SST trends have likely contributed to the drying in Chile, in agreement with Garreaud et al. (2020). Elsewhere, SST impacts appear small, though Mediterranean SST warming may have offset drying (in contrast to findings in Hoerling et al. (2012)). However, our analysis relies on only one set of AMIP simulations from CESM, and a more detailed analysis of multiple AMIP simulations and of tropical versus extratropical SSTs would allow for more robust results. Furthermore, the tropical Pacific is known to affect the SAM (Karoly, 1989; Q. Ding et al., 2012; H. Ding et al., 2015), so more research is needed to understand how our Southern Hemisphere MC results are impacted by SST trends.

Data Availability Statement

ECMWF Reanalysis v5 (ERA5) data used in this study are available at Hersbach et al. (2023). Climatic Research Unit Time Series (CRU-TS) data are available at https://crudata.uea.ac.uk/cru/data/hrg/cru_ts_4.07/ (Harris et al., 2020). Global Precipitation Climatology Project (GPCP) data are available at https://psl.noaa.gov/data/gridded/data.gpcp.html (Adler et al., 2003) Community Earth System Model version 2 (CESM) Large Ensemble data are available at https://climatedata.ibs.re.kr/data/cesm2-lens. MPI-ESM1.2-LR data and SMHI-LENS EC-Earth3 data are available at https://aims2.llnl.gov/ (Deser et al., 2020; Rodgers et al., 2021; Wyser et al., 2021). CAM6 Prescribed SST AMIP Ensembles are available at https://www.cesm.ucar.edu/working-groups/climate/simulations/cam6-prescribed-sst (Phillips & Simpson, 2024). GPCC (Global Precipitation Climatology Center) data are available at Schneider et al. (2022). E-OBS version 31.0e data are available at https://www.ecad.eu/download/ensembles/download.php (Cornes et al., 2018).

Acknowledgments
We thank Matt Patterson for his assistance in understanding the circulation analogs technique. This study was supported by NERC Award NE/S007474/1. We also thank two anonymous reviewers for their constructive comments.

References

Adams, D. K., & Comrie, A. C. (1997). The North American monsoon. *Bulletin of the American Meteorological Society*, *78*(10), 2197–2214. https://doi.org/10.1175/1520-0477(1997)078<2197:tnam>2.0.co;2

Adler, R. F., Huffman, G. J., Chang, A., Ferraro, R., Xie, P.-P., Janowiak, J., et al. (2003). The version-2 global precipitation climatology project (GPCP) monthly precipitation analysis (1979–present). *Journal of Hydrometeorology*, *4*(6), 1147–1167. https://doi.org/10.1175/1525-7541(2003)004<1147:tvgpcp>2.0.co;2

Alessi, M. J., & Rugenstein, M. (2024). Potential near-term wetting of the Southwestern United States if the Eastern and Central Pacific cooling trend reverses. *Geophysical Research Letters*, *51*(13), e2024GL108292. https://doi.org/10.1029/2024GL108292

Barlow, M., Nigam, S., & Berbery, E. H. (1998). Evolution of the North American monsoon system. *Journal of Climate*, *11*(9), 2238–2257. https://doi.org/10.1175/1520-0442(1998)011<2238:eotnam>2.0.co;2

Beck, H. E., Zimmermann, N. E., McVicar, T. R., Vergopolan, N., Berg, A., & Wood, E. F. (2018). Present and future Köppen-Geiger climate classification maps at 1-km resolution. *Scientific Data*, *5*(1), 1–12.

Boisier, J. P., Alvarez-Garreton, C., Cordero, R. R., Damiani, A., Gallardo, L., Garreaud, R. D., et al. (2018). Anthropogenic drying in central-southern Chile evidenced by long-term observations and climate model simulations. *Elementa: Science of the Anthropocene*, *6*, 74. https://doi.org/10.1525/elementa.328

Boisier, J. P., Rondanelli, R., Garreaud, R. D., & Muñoz, F. (2016). Anthropogenic and natural contributions to the Southeast Pacific precipitation decline and recent megadrought in Central Chile. *Geophysical Research Letters*, *43*(1), 413–421. https://doi.org/10.1002/2015GL067265

Byrne, M. P., & O'Gorman, P. A. (2015). The response of precipitation minus evapotranspiration to climate warming: Why the "wet-get-wetter, dry-get-drier" scaling does not hold over land. *Journal of Climate*, *28*(20), 8078–8092. https://doi.org/10.1175/JCLI-D-15-0369.1

Campos, D., & Rondanelli, R. (2023). ENSO-related precipitation variability in Central Chile: The role of large scale moisture transport. *Journal of Geophysical Research: Atmospheres*, *128*(17), e2023JD038671. https://doi.org/10.1029/2023JD038671

Carleton, A. M., Carpenter, D. A., & Weser, P. J. (1990). Mechanisms of interannual variability of the southwest United States summer rainfall maximum. *Journal of Climate*, *3*(9), 999–1015. https://doi.org/10.1175/1520-0442(1990)003<0999:moivot>2.0.co;2

Coburn, J., & Pryor, S. C. (2021). Differential credibility of climate modes in CMIP6. *Journal of Climate*, *34*(20), 8145–8164. https://doi.org/10.1175/jcli-d-21-0359.1

Cornes, R. C., Van Der Schrier, G., Van Den Besselaar, E. J., & Jones, P. D. (2018). An ensemble version of the E-OBS temperature and precipitation data sets. *Journal of Geophysical Research: Atmospheres*, *123*(17), 9391–9409. https://doi.org/10.1029/2017jd028200

Deser, C., Lehner, F., Rodgers, K. B., Ault, T., Delworth, T. L., DiNezio, P. N., et al. (2020). Insights from Earth system model initial-condition large ensembles and future prospects. *Nature Climate Change*, *10*(4), 277–286. https://doi.org/10.1038/s41558-020-0731-2

Deser, C., & Phillips, A. S. (2023). A range of outcomes: The combined effects of internal variability and anthropogenic forcing on regional climate trends over Europe. *Nonlinear Processes in Geophysics*, *30*(1), 63–84. (Publisher: Copernicus Publications). https://doi.org/10.5194/npg-30-63-2023

Deser, C., Terray, L., & Phillips, A. S. (2016). Forced and internal components of winter air temperature trends over North America during the past 50 years: Mechanisms and implications. *Journal of Climate*, *29*(6), 2237–2258. https://doi.org/10.1175/JCLI-D-15-0304.1

Ding, H., Greatbatch, R. J., & Gollan, G. (2015). Tropical impact on the interannual variability and long-term trend of the Southern Annular Mode during austral summer from 1960/1961 to 2001/2002. *Climate Dynamics*, *44*(7), 2215–2228. https://doi.org/10.1007/s00382-014-2299-x

Ding, Q., Steig, E. J., Battisti, D. S., & Wallace, J. M. (2012). Influence of the tropics on the southern annular mode. *Journal of Climate*, *25*(18), 6330–6348. https://doi.org/10.1175/JCLI-D-11-00523.1

Fogt, R., & Marshall, G. (2020). The southern annular mode: Variability, trends, and climate impacts across the Southern Hemisphere. *Wiley Interdisciplinary Reviews: Climate Change*, *11*(4). https://doi.org/10.1002/wcc.652

Garreaud, R. D., Boisier, J. P., Rondanelli, R., Montecinos, A., Sepúlveda, H. H., & Veloso-Aguila, D. (2020). The Central Chile Mega Drought (2010–2018): A climate dynamics perspective. *International Journal of Climatology*, *40*(1), 421–439. https://doi.org/10.1002/joc.6219

Garreaud, R. D., Clem, K., & Veloso, J. V. (2021). The South Pacific pressure trend dipole and the southern blob. *Journal of Climate*, *34*(18), 7661–7676. https://doi.org/10.1175/jcli-d-20-0886.1

Gillett, N. P., Kell, T. D., & Jones, P. (2006). Regional climate impacts of the southern annular mode. *Geophysical Research Letters*, *33*(23). https://doi.org/10.1029/2006gl027721

Guo, R., Deser, C., Terray, L., & Lehner, F. (2019). Human influence on winter precipitation trends (1921–2015) over North America and Eurasia revealed by dynamical adjustment. *Geophysical Research Letters*, *46*(6), 3426–3434. https://doi.org/10.1029/2018GL081316

Harris, I., Osborn, T. J., Jones, P., & Lister, D. (2020). Version 4 of the CRU TS monthly high-resolution gridded multivariate climate dataset [Dataset]. *Scientific Data*, *7*(1), 109. https://doi.org/10.1038/s41597-020-0453-3

Harvey, B., Hawkins, E., & Sutton, R. (2023). Storylines for future changes of the North Atlantic jet and associated impacts on the UK. *International Journal of Climatology*, *43*(10), 4424–4441. https://doi.org/10.1002/joc.8095

Held, I. M., & Soden, B. J. (2006). Robust responses of the hydrological cycle to global warming. *Journal of Climate*, *19*(21), 5686–5699. https://doi.org/10.1175/JCLI3990.1

Hersbach, H., Bell, B., Berrisford, P., Biavati, G., Horányi, A., Muñoz Sabater, J., et al. (2023). ERA5 monthly averaged data on single levels from 1940 to present [Dataset]. *Copernicus Climate Change Service (C3S) Climate Data Store (CDS)*. https://doi.org/10.24381/cds.f17050d7

Hessl, A., Allen, K., Vance, T., Abram, N., & Saunders, K. (2017). Reconstructions of the southern annular mode (SAM) during the last millennium. *Progress in Physical Geography*, *41*(6), 834–849. https://doi.org/10.1177/0309133317743165

Hoerling, M., Eischeid, J., Perlwitz, J., Quan, X., Zhang, T., & Pegion, P. (2012). On the increased frequency of Mediterranean drought. *Journal of Climate*, *25*(6), 2146–2161. https://doi.org/10.1175/jcli-d-11-00296.1

Jones, P. D., & Lister, D. H. (2007). Intercomparison of four different Southern Hemisphere sea level pressure datasets. *Geophysical Research Letters*, *34*(10). https://doi.org/10.1029/2007GL029251

Karoly, D. J. (1989). Southern Hemisphere circulation features associated with El Niño-Southern Oscillation Events. *Journal of Climate*, *2*(11), 1239–1252. https://doi.org/10.1175/1520-0442(1989)002⟨1239:SHCFAW⟩2.0.CO;2

Kelley, C., Ting, M., Seager, R., & Kushnir, Y. (2012). The relative contributions of radiative forcing and internal climate variability to the late 20th century winter drying of the Mediterranean region. *Climate Dynamics*, *38*(9–10), 2001–2015. https://doi.org/10.1007/s00382-011-1221-z

Kosaka, Y., Kobayashi, S., Harada, Y., Kobayashi, C., Naoe, H., Yoshimoto, K., et al. (2024). The JRA-3Q reanalysis. *Journal of the Meteorological Society of Japan Series II*, *102*(1), 49–109. https://doi.org/10.2151/jmsj.2024-004

Lehner, F., Deser, C., Simpson, I. R., & Terray, L. (2018). Attributing the U.S. Southwest's recent shift into drier conditions. *Geophysical Research Letters*, *45*(12), 6251–6261. https://doi.org/10.1029/2018GL078312

Lim, E.-P., Hendon, H. H., Arblaster, J. M., Delage, F., Nguyen, H., Min, S.-K., & Wheeler, M. C. (2016). The impact of the southern annular mode on future changes in Southern Hemisphere rainfall. *Geophysical Research Letters*, *43*(13), 7160–7167. https://doi.org/10.1002/2016GL069453

Marshall, G. (2003). Trends in the southern annular mode from observations and reanalyses. *Journal of Climate*, *16*(24), 4134–4143. https://doi.org/10.1175/1520-0442(2003)016⟨4134:TITSAM⟩2.0.CO;2

Meneghini, B., Simmonds, I., & Smith, I. N. (2007). Association between Australian rainfall and the southern annular mode. *International Journal of Climatology: A Journal of the Royal Meteorological Society*, *27*(1), 109–121. https://doi.org/10.1002/joc.1370

Montecinos, A., & Aceituno, P. (2003). Seasonality of the ENSO-related rainfall variability in central Chile and associated circulation anomalies. *Journal of Climate*, *16*, 281–296. https://doi.org/10.1175/1520-0442(2003)016⟨0281:SOTERR⟩2.0.CO;2

Olonscheck, D., Suarez-Gutierrez, L., Milinski, S., Beobide-Arsuaga, G., Baehr, J., Fröb, F., et al. (2023). The new Max Planck institute grand ensemble with CMIP6 forcing and high-frequency model output. *Journal of Advances in Modeling Earth Systems*, *15*(10), e2023MS003790. https://doi.org/10.1029/2023ms003790

O'Reilly, C. H., Woollings, T., & Zanna, L. (2017). The dynamical influence of the Atlantic multidecadal oscillation on continental climate. *Journal of Climate*, *30*(18), 7213–7230. https://doi.org/10.1175/jcli-d-16-0345.1

Parker, T., & Gallant, A. J. (2022). The role of heavy rainfall in drought in Australia. *Weather and Climate Extremes*, *38*, 100528. https://doi.org/10.1016/j.wace.2022.100528

Pascale, S., Kapnick, S. B., Delworth, T. L., & Cooke, W. F. (2020). Increasing risk of another Cape Town "Day Zero" drought in the 21st century. *Proceedings of the National Academy of Sciences of the United States of America*, *117*(47), 29495–29503. https://doi.org/10.1073/pnas.2009144117

Phillips, A., & Simpson, I. (2024). CAM6 prescribed SST AMIP ensembles [Dataset]. *Boulder, CO: Research Data Archive at the National Center for Atmospheric Research, Computational and Information Systems Laboratory*. https://doi.org/10.26024/800d-nj44

Polade, S. D., Gershunov, A., Cayan, D. R., Dettinger, M. D., & Pierce, D. W. (2017). Precipitation in a warming world: Assessing projected hydro-climate changes in California and other Mediterranean climate regions. *Scientific Reports*, *7*(1), 10783. https://doi.org/10.1038/s41598-017-11285-y

Reyes-García, P., & Jofré, D. (2024). Acciones climáticas frente a la sequía severa: el caso de comunidades rurales costeras del chile central. *Íconos-Revista de Ciencias Sociales*, (79), 185–205.

Rodgers, K. B., Lee, S.-S., Rosenbloom, N., Timmermann, A., Danabasoglu, G., Deser, C., et al. (2021). Ubiquity of human-induced changes in climate variability. *Earth System Dynamics*, *12*(4), 1393–1411. https://doi.org/10.5194/esd-12-1393-2021

Schneider, U., Hänsel, S., Finger, P., Rustemeier, E., & Ziese, M. (2022). GPCC full data monthly product version 2022 at 0.5°: Monthly land-surface precipitation from rain-Gauges built on GTS-based and historical data [Dataset]. *Deutscher Wetterdienst (DWD)*. https://doi.org/10.5676/DWD_GPCC/FD_M_V2022_050

Seager, R., Henderson, N., & Cane, M. (2022). Persistent discrepancies between observed and modeled trends in the tropical Pacific Ocean. *Journal of Climate*, *35*(14), 4571–4584. https://doi.org/10.1175/jcli-d-21-0648.1

Seager, R., Osborn, T. J., Kushnir, Y., Simpson, I. R., Nakamura, J., & Liu, H. (2019). Climate variability and change of Mediterranean-type climates. *Journal of Climate*, *32*(10), 2887–2915. https://doi.org/10.1175/JCLI-D-18-0472.1

Seager, R., Wu, Y., Cherchi, A., Simpson, I. R., Osborn, T. J., Kushnir, Y., et al. (2024). Recent and near-term future changes in impacts-relevant seasonal hydroclimate in the world's Mediterranean climate regions. *International Journal of Climatology*, *44*(11), 3792–3820. https://doi.org/10.1002/joc.8551

Shepherd, T. G. (2014). Atmospheric circulation as a source of uncertainty in climate change projections. *Nature Geoscience*, *7*(10), 703–708. https://doi.org/10.1038/ngeo2253

Simpson, I. R., Bacmeister, J., Neale, R. B., Hannay, C., Gettelman, A., Garcia, R. R., et al. (2020). An evaluation of the large-scale atmospheric circulation and its variability in CESM2 and other CMIP models. *Journal of Geophysical Research: Atmospheres*, *125*(13), e2020JD032835. https://doi.org/10.1029/2020JD032835

Sippel, S., Meinshausen, N., Merrifield, A., Lehner, F., Pendergrass, A. G., Fischer, E., & Knutti, R. (2019). Uncovering the forced climate response from a single ensemble member using statistical learning. *Journal of Climate*, *32*(17), 5677–5699. https://doi.org/10.1175/JCLI-D-18-0882.1

Tortajada, C., Kastner, M. J., Buurman, J., & Biswas, A. K. (2017). The California drought: Coping responses and resilience building. *Environmental Science & Policy*, *78*, 97–113. https://doi.org/10.1016/j.envsci.2017.09.012

Velasquez-Jimenez, L., & Abram, N. (2023). Technical note: A best-practice approach to calculating the southern annular mode index. *Climate of the Past*, *20*(5), 1125–1139. https://doi.org/10.5194/cp-20-1125-2024

Wang, H., & Kumar, A. (2015). Assessing the impact of ENSO on drought in the U.S. southwest with NCEP climate model simulations. *Journal of Hydrology*, *526*, 30–41. https://doi.org/10.1016/J.JHYDROL.2014.12.012

Waugh, D. W., Banerjee, A., Fyfe, J. C., & Polvani, L. M. (2020). Contrasting recent trends in southern hemisphere westerlies across different ocean basins. *Geophysical Research Letters*, *47*(18), e2020GL088890. https://doi.org/10.1029/2020gl088890

Wills, R. C., Dong, Y., Proistosecu, C., Armour, K. C., & Battisti, D. S. (2022). Systematic climate model biases in the large-scale patterns of recent sea-surface temperature and sea-level pressure change. *Geophysical Research Letters*, *49*(17), e2022GL100011. https://doi.org/10.1029/2022gl100011

Woollings, T., Drouard, M., O'Reilly, C. H., Sexton, D. M., & McSweeney, C. (2023). Trends in the atmospheric jet streams are emerging in observations and could be linked to tropical warming. *Communications Earth & Environment*, *4*(1), 125. https://doi.org/10.1038/s43247-023-00792-8

Wyser, K., Koenigk, T., Fladrich, U., Fuentes-Franco, R., Karami, M. P., & Kruschke, T. (2021). The SMHI large ensemble (SMHI-LENS) with EC-EARTH3. 3.1. *Geoscientific Model Development*, *14*(7), 4781–4796. https://doi.org/10.5194/gmd-14-4781-2021

References From the Supporting Information

Horowitz, R. L., McKinnon, K. A., & Simpson, I. R. (2022). Circulation and soil moisture contributions to heatwaves in the United States. *Journal of Climate*, *35*(24), 8031–8048. https://doi.org/10.1175/JCLI-D-21-0156.1